HEDL-SA-2146

NUCLEAR DATA RELEVANT TO SHIELD DESIGN OF FMIT FACILITY

L. L. Carter, R. J. Morford, and A. D. Wilcox

Hanford Engineering Development Laboratory
Richland, Washington 99352, U.S.A.

ABSTRACT

Nuclear data requirements are reviewed for the design of the Fusion Materials Irradiation Test (FMIT) facility. This accelerator-based facility, now in the early stages of construction at Hanford, will provide high fluences in a fusion-like radiation environment for the testing of materials. The nuclear data base required encompasses the entire range of neutron energies from thermal to 50 MeV. In this review, we consider neutron source terms, cross sections for thermal and bulk shield design, and neutron activation for the facility.

INTRODUCTION

The FMIT facility [1] will provide the only high-fluence data for a fusion-like radiation environment during the next decade. Groundbreaking ceremonies were held February 22, 1980 to start construction of this accelerator-based facility at Hanford with completion scheduled for 1984.

The neutron source, produced by a 0.1 Amp beam of 35 MeV deuterons incident upon a flowing lithium target, is highly anisotropic with a rapid spectral variation with angle. The spectrum in the forward direction is characterized by a broad peak around ∿14 MeV with a high energy tail extending to ∿50 MeV. While the broad peak provides the major portion of the source for material damage studies, the contribution from somewhat higher energy neutrons is also important and the extreme high energy portion of the tail impacts shield design.

An adequate design of the facility requires knowledge of the (d,Li) neutron source distribution, neutron cross section data from 20 to 50 MeV (in addition to libraries such as ENDF/B below 20 MeV) for the major isotopic constituents of the shields, extensive neutron activation cross section data, and deuteron activation cross sections along with beam loss criteria within the

DISCLAIMER

accelerator. Integral measurements of neutron and deuteron activation also play an important role. General nuclear data requirements were considered during the previous symposium [2] for (d,Be) and (d,Li) based neutron sources. This session of the current symposium will focus specifically upon the FMIT facility. In this review paper, nuclear data relative to shield design will be considered while the next review paper [3] will focus upon irradiation damage.

NEUTRON SOURCE CHARACTERISTICS

Both shield design and a proper understanding of the material damage of irradiated test specimens require an experimental determination of the neutron source spectrum resulting from 35 MeV deuterons incident upon lithium. From a shielding point of view, there was an early interest in the shape of the high energy tail since there were theoretical reasons to believe that the $^{7}Li(d,n)^{8}Be$ reaction with a Q value of 15 MeV could lead to neutrons with energies up to ~50 MeV. Transport calculations [4,5] indicated that such neutrons would severely impact shield design even if source strengths were down by two orders of magnitude from the peak around 14 MeV.

The (d,Li) source has been characterized by thick target measurements [6] for ten different angles using time-of-flight techniques and the cyclotron at the University of California at Davis. The spectra at the four angles of Figure 1 (measured data [6] without smoothing) are shown to illustrate neutron energy regimes that impact various aspects of shield design. Particularly significant is the shoulder from 30 to 45 MeV at eight degrees arising from the Q value of 15 MeV. This shoulder is prominent from about six to twenty degrees.

The 35 MeV deuterons impinge upon a flowing lithium target positioned within a 5'x8'x6' test cell (see Figures 2a & 2b). The shoulder in the neutron spectra beyond 30 MeV at forward angles is important for a determination of the shield thickness of the back wall of the test cell since these source neutrons are the dominant neutrons that penetrate the shield. For side walls, the source neutrons between 20 and 40 MeV dominate. This is not to say, however, that the lower energy portion of the spectrum can be ignored in all aspects of shield design. The lower energy neutrons must be considered in the design of the thermal shield and in nuclear heat deposition within the test cell since a low energy neutron has the potential for depositing ~8 MeV of energy via capture. The entire neutron energy regime is potentially important for neutron activation and must be properly treated to determine shield requirements for positioning and removal of test specimens, maintenance of the accelerator system, and activation of coolants and atmospheres.

The neutron source within the Linear Accelerator (LINAC) and beam transport areas arises from stray deuterons incident upon

materials such as Fe, Cu, Au and Al. While the neutron source strength per unit of deuteron current is less for these materials than for lithium, the general neutron energy regime of Figure 1 is still applicable at the high energy portion of the accelerator. Uncertainties in dose levels within the LINAC, due to both neutron and deuteron activation, are currently dominated by uncertainties in deuteron losses rather than by (d,X) source data or by neutron activation cross sections.

BULK SHIELD DESIGN

Transport calculations have validated the concept presented by a simple removal-theory model of high energy (20-50 MeV) neutron transport through shields. A simple model enables first-order comparisons of shields — both modular and homogeneous — and gives some insights into sensitivities of the dose through the shield to cross section data. Of course, rigorous transport calculations are made to verify the more crucial conclusions.

In the following discussion the outer portion of the shield is assumed to contain enough hydrogenous material so that once the neutron energy is reduced below about one MeV it is rapidly thermalized and captured. A simplified pictorial of the penetration of a high energy neutron source through the shield is shown in Figure 3. Most of the neutrons that eventually emerge from the shield either have a very long first flight, which takes them nearly through the shield, or else suffer one or more small-angle elastic collisions (typically with long flight paths between collisions) before penetrating through most (or all) of the shield. In contrast, neutrons which suffer wide angle collisions prior to deep penetration must travel many more mean free paths or scatter back into the appropriate small solid angle. The neutrons that suffer nonelastic collisions usually lose enough energy so that their probability of penetrating the shield is substantially reduced irrespective of scattering angle.

The microscopic removal cross section is defined as

$$\sigma_r(E) = \sigma_{non}(E) + \alpha\, \sigma_{el}(E) \ , \qquad (1)$$

where $\sigma_{non}(E)$ is the nonelastic cross section, $\sigma_{el}(E)$ is the elastic cross section, and α is the fraction of the elastically scattered neutrons suffering a wide angle ($\gtrsim 25°$) deflection. Such a removal cross section is compared in Figure 4 for iron with two different cross section evaluations. The removal cross section labeled "MCNP" was calculated with Eq. (1) using as a data base the pointwise cross section library that is currently being used for shield design with the Monte Carlo code, MCNP [7,8]. The lower curve was obtained by folding experimental data [9,10] and a priori data using a generalized least squares procedure.

Both removal cross section evaluations of Figure 4 decrease monotonically with increasing neutron energy. Although the

decrease is small, it is important since the macroscopic removal cross section is applied exponentially: the dose through a homogeneous shield of thickness x is approximately

$$D = C \int S(E)\, e^{-\Sigma_r(E)x}\, dE \,, \qquad (2)$$

where S(E) is the energy dependent source and C is a constant for a given shield material. The exponential enhances the worth of the higher energy source neutrons (E>30 MeV) incident upon the back wall so that they are the dominant neutrons that penetrate the thick back wall shield. This is illustrated by the curves in Figure 5 for neutron transport through an eight foot slab of high density magnetite concrete.

The solid (importance) curve in Figure 5 was generated with Monte Carlo calculations [4,11]. A point on the curve gives the dose through eight feet of high density concrete due to a one neutron per cm^2 normally incident source with kinetic energy given by the abscissa. For example, a 40 MeV source neutron is ~250 times as important as a 20 MeV source neutron. Folding this curve with the FMIT spectrum incident upon the back wall results in the future contribution [12] (sometimes called contributon current) curve of Figure 5; i.e., the product of the dose through the slab for unit monoenergetic sources with the source intensity. For the relatively thin eight foot shield, the contributon current at 40 MeV is about seven times that of 20 MeV.

Transport calculations have verified the removal theory interpretation that the nonelastic cross section above 20 MeV is the most sensitive of the nuclear data for bulk shielding. Somewhat less important is the elastic cross section and its associated angular distribution. Even though the elastic cross section is very forward peaked above 20 MeV, treating it as straight ahead results in an overconservatism of at least two orders of magnitude in the dose for the back wall shield thicknesses of interest.

The dose through bulk shields is not very sensitive to the energy- and angular-distribution of neutrons from nonelastic events; however, calculations of neutron flux fields within test assemblies could be sensitive to these distributions. Previous studies [5] have shown that gamma production cross sections for neutron energies above 20 MeV may be neglected in the design of bulk shields. Further confirmation of this is desirable.

The most important elements for the bulk shield analysis are basically the constituents of concrete and iron shields. First priority in nuclear data needs is assigned to iron and oxygen with second priority given to silicon, calcium, and carbon. Recent measurements have been made of the total, nonelastic, and removal cross sections at 40 and 50 MeV [9]. The experimental data points shown in Figure 4 for iron aided in obtaining an updated evaluation of the removal and nonelastic cross sections and assignment of uncertainties in the energy range 20-50 MeV. Better agreement

between the pointwise library being used in the MCNP Monte Carlo code and new evaluations based upon the measurements was obtained for oxygen, calcium, and carbon. Hence our confidence in the nuclear data for these elements has been improved, but much work remains to be done to obtain overall satisfactory agreement between nuclear model codes and experimental data.

TRANSPORT CROSS SECTION LIBRARIES FOR FMIT

The two cross section libraries that are being used in the transport calculations for FMIT are summarized in Figure 6. The pointwise Monte Carlo library is based upon ENDF/B-IV below 20 MeV. Cross sections from 20 to 60 MeV were appended to this library [4, 13] for the elements H, C, O, Si, Ca, Cr, Fe, and Ni using available nuclear data. Nonelastic cross sections from 20 to 60 MeV were taken directly as those recommended by Wilson [14]. Intranuclear-cascade plus Evaporation (IC+E) model calculations [15] at Oak Ridge National Laboratory (ORNL) were used for the number of secondary neutrons from nonelastic scattering events and their energy and angular distributions. Optical model calculations at Hanford Engineering Development Laboratory (HEDL), checked against available experimental data, were used to obtain the elastic scattering cross sections and their angular distributions. An exception is hydrogen, which is based entirely upon experimental measurements.

The coupled neutron-gamma multigroup cross section library is currently being used primarily in one-dimensional discrete ordinates calculations. This library [16] was constructed by Alsmiller and Barish at ORNL by appending multigroup cross sections between 14.9 and 60 MeV to an existing RSIC fusion library [17] for energies below 14.9 MeV. The cross sections above 14.9 MeV are P_5 and, hence, include an adequate expansion for deep penetration calculations. The nonelastic and elastic cross sections above 14.9 MeV were based upon optical model calculations checked against available measurements, while the nonelastic energy and angular distributions were based upon the IC+E model calculations [15]. The fusion cross section library below 14.9 MeV was for infinite dilution. Resonance self-shielding corrections have been made at HEDL to obtain another 0-60 MeV library for iron.

NUCLEAR HEAT DEPOSITION

Nuclear heat deposition from neutron and gamma interactions is important within the material test modules, the thermal shield walls of the test cell (see Figure 2b), and the bulk shield beyond the thermal shield. Calculations of heat deposition are sensitive to neutron transport, neutron KERMA factors, and gamma production cross sections. Nuclear data limitations have been experienced for all three of these categories. The most important element is

iron, although nickel, chromium, calcium, silicon, oxygen, and hydrogen impact various calculations.

Unfortunately, energy balances in ENDF/B continue to have shortcomings for the generation of cross section libraries and for the calculation of KERMA factors [18]. Corrections in the MCNP library have been made over various energy regimes for the more important elements. Los Alamos Scientific Laboratory (LASL) has improved gamma production and energy balances in a new cross section evaluation for iron [19]. This is currently being processed for inclusion in the MCNP master library.

Integral tests of the neutron transport are necessary to establish confidence in the heat deposition calculations. An important example is the back wall of the test cell. The current design of the thermal shield requires about 24 inches of iron and graphite and an inch or two of Boral. Interspaced in this ∿26 inches are some channels for gas cooling of the wall. The bulk shield of concrete is beyond this thermal shield, and an important parameter is the heat deposition within the concrete. This heat deposition is reduced to an acceptable level by an appropriate thermal shield design.

The heat deposition within the concrete is sensitive to the proper treatment of the higher energy (∿14 MeV) neutrons within the thermal shield. This includes (n,2n) and (n,3n) interactions. An integral measurement of the transmission of (d,Li) neutrons through an iron block has recently been made by HEDL to check calculational capabilities [20].

NEUTRON STREAMING

Penetrations through the test cell walls and through the walls of the accelerator require assessments of neutron streaming. Experience to date indicates that calculations of streaming are limited more by geometry models and the two- and three-dimensional aspects of the problem than by nuclear data [11]. The energy regime above 20 MeV has less of an impact upon the results than is true for bulk shields.

ACTIVATION

Approach

Both neutron and deuteron induced activation must be included in the overall assessments for the FMIT facility. Deuteron induced activation is primarily dealt with experimentally as described in a paper of this session [20]. The broader area of neutron activation is treated calculationally and, as the calculations indicate sensitive areas, will include some integral measurements.

The nuclear data base, along with computer codes and linkages, is used to treat neutron activation problems with the general

problem flow shown in Figure 7. The activation problem of concern is first defined. These include the LINAC accelerator with hands-on maintenance being highly desirable, the beam transport area, and activation of the test cell equipment, test cell walls, test assemblies, and the atmosphere within the accelerator and the test cell. After an area of concern is defined, the dozens of possible reactions are sifted through to isolate the most important reactions based upon half-lives, the decay energies of the gamma-rays, and conservative estimates of the relevant cross sections. If cross sections for the most important reactions are not included in the FMIT neutron multigroup activation library, the library is updated. Most of the data in the FMIT activation library has been generated using ENDF/B-V data (when it exists) along with a modified version of THRESH [21]. The modification made at HEDL extends the output of THRESH to 40 MeV with normalization to the ENDF/B-V data at 20 MeV whenever possible.

The energy dependent neutron flux is folded with the cross sections in the activation library to obtain gamma-ray source terms. The resulting gamma flux field is invariably dominated by only a few of the neutron reaction modes for the cooling times of interest. Cross sections for these reaction modes are examined to determine whether there is a need for further refinements. Refinements include the utilization of more exact numerical calculations of the cross sections, with codes such as HAUSER [22], and/or integral measurements of neutron activation.

The activation calculations summarized in the following sections utilized the atom densities shown in Table I and are based upon a one year irradiation at a 0.1 Amp deuteron current. A summary of important reactions is given in Table II.

Neutron Activation of Stainless Steel Within Test Cell

Stainless steel is a very important material since it will be used both structurally and as a major component for the material test modules. Calculations of stainless steel neutron activation have been made for targets located within the prime test region and for various other positions within the test cell.

The summary in Table III gives the volume averaged activation for a 5.5 x 4.0 x 5.0 cm parallelepiped of stainless steel placed within the pristine flux field of the prime test region (see Figure 2b for location and Table I for stainless steel composition). The most important radionuclide for shield design is ^{56}Co because of its hard 3.26 MeV gamma rays and its half-life of 77 days. This leads to a requirement for $\sim$12 inches of lead in the cask for transporting the irradiated test modules.

The most important reactions for activation of stainless steel within the prime test region are ^{58}Ni(n,t)^{56}Co and ^{58}Ni(n,nd)^{56}Co. For cooling times less than a few hours, ^{56}Fe(n,p)^{56}Mn will also be important in some shielding applications. At wide-angle positions within the test cell, the spectra is softer and the concentration of ^{56}Co relative to the other

isotopes will decrease by nominally a factor of four from that of Table III.

Neutron Activation of Important Elements Within Prime Test Volume

The volume averaged pristine neutron flux field, within a 5.5 x 4.0 x 5.0 cm parallelepiped positioned within the prime test region, was also folded with activation cross sections for various elements of interest. The results summarized in Table IV were obtained using the theoretical atom densities of Table I. Since the activities of Tables III and IV were generated using the pristine flux field, extrapolations to configurations with enough material to significantly perturb the flux should be made with care.

Neutron Activation of Aluminum Beam Tube

Neutron streaming back down the beam tube from the lithium target is the dominant mode of neutron activation of the beam tube near the test cell where access to the magnet is essential. An analysis was made to determine the possible advantage of utilizing aluminum rather than stainless steel for the beam tube. The measured neutron spectrum [6] at 150° for a (d,Li) source was used to compare these activations.

The most important radionuclides for the aluminum beam tube were found to be ^{24}Na, ^{65}Zn, ^{46}Sc, ^{60}Co, and ^{48}Sc. The major reaction modes are given in Table II. About one week after shutdown the ^{24}Na will decay to the point where the longer lived nuclides will dominate. Of these, only ^{48}Sc will decay appreciably for the maintenance times of concern.

The overall conclusion is that the aluminum does have advantages over stainless steel, from an activation viewpoint, for cooling time beyond the first few days.

Neutron Activation Along LINAC

Even though deuteron losses are greater at the lower energy end of the accelerator, neutron activation problems are more acute at the higher energy end because the generation rate of neutrons per lost deuteron increases rapidly with increasing deuteron energy. Roughly the same neutron energy regime is of concern along the high energy portion of the accelerator and beam transport area as in the test cell. However, because of the rapid decrease in the neutron source strength beyond ~20 MeV, activation at energies above ~30 MeV may usually be neglected. For wide angles, such as side-on at 90 degrees, a 20 MeV limit is usually adequate.

Neutron flux levels within the LINAC were determined from a Monte Carlo calculation [11] with a model of the geometry that included the last ten drift tubes. The results of folding the cross sections of the FMIT activation library with the neutron flux at the high energy end of the accelerator are given in Tables V and

VI for the accelerator tunnel concrete walls and for the LINAC, respectively.

The most important gamma-ray source within the concrete is from ^{24}Na for cooling times beyond a few hours; ^{56}Mn is also important for short cooling times. Since most of the ^{24}Na and ^{56}Mn nuclides are generated by thermal neutrons, a reduction of the gamma field within the accelerator tunnel is obtainable by simply borating the concrete of the LINAC walls.

The neutron activation summary of Table VI includes materials within the drift tubes and the outer tank wall of the accelerator. Point kernel calculations, using appropriate volume weighted source terms for the various materials, were made to obtain radiation fields along the high energy portion of the accelerator tunnel. A dose rate of 4 mrem/hr, at a distance of one foot from the tank, was obtained for a cooling time of one day. This does not include the contribution from the concrete walls of ∿5 mrem/hr. This component from the concrete walls can be reduced nearly an order of magnitude by borating the concrete. The dose rate scales linearly with the deuteron loss — assumed to be 3μAmp/m on gold.

This iteration did not include the water coolant of the drift tubes in the model of the geometry for the Monte Carlo calculation of neutron flux levels. An inclusion of the water is expected to increase the thermal flux with a corresponding increase from low energy reaction modes. The 2.6 hour half-life radionuclide ^{56}Mn, from $^{55}Mn(n,\gamma)^{56}Mn$, is expected to increase significantly with an appropriate treatment of the thermal flux.

Air Within Accelerator Tunnel

Preliminary assessments have been made of the activation of air within the accelerator tunnel. The radionuclides of most concern from a maximum permissible concentration (MPC) standpoint are ^{13}N, ^{16}N, ^{14}C, ^{39}Ar, and ^{41}Ar. The important reactions are summarized in Table II.

Experimenters Side Wall

Activation assessments are sometimes sensitive to the neutron transport calculations. An example is the test cell side wall containing plugs for experimental access. Nuclide activation beyond the first ∿4 feet of this iron-dominated shield are of concern. Here the flux levels depend upon an appropriate calculation of the transport and slowing down of the higher energy neutrons and the subsequent transport of the lower energy neutrons. There is a wealth of experimental and calculational [13] results for neutron transport within the iron resonance region (20 keV to 2 MeV). An integral measurement [20] of the transmission of (d,Li) neutrons through an iron block has now provided experimental data at higher energies.

SUMMARY

Discrete ordinates and Monte Carlo codes, developed for applications in nuclear reactors, fusion systems, and weapons physics, are applicable for solving neutron and photon transport problems relative to the FMIT facility. Extension of the nuclear data base is a challenging problem. This encompasses the appropriate cross sections for the neutron transport for the energy range 0 to 50 MeV and neutron activation cross sections for dozens of reaction modes over the energy range 0 to ∿30 MeV.

A pointwise library and a multigroup library have been developed for the Monte Carlo and discrete ordinates calculations. These neutron and gamma-ray transport libraries include the neutron energy regime 0 to 60 MeV for the most important elements used in the FMIT facility. Both libraries include adequate angular resolution to serve as data bases for deep penetration calculations. Sensitivity calculations have isolated the nonelastic cross section between 20 and 50 MeV as the most important cross section for the bulk shield design. Next in importance is the elastic scattering cross section for the same energy range with its corresponding angular distribution. Cross section measurements at 40 and 50 MeV for iron, oxygen, calcium, and carbon have enabled improved normalizations of optical model calculations.

A multigroup neutron activation library for FMIT has been created at HEDL. Because of the many reaction modes possible at the high neutron energies, the completeness of the library is examined prior to each calculation involving new isotopes. The dozens of possible reaction modes are sifted through to isolate the most important reactions by examining half-lives, decay energies of the gamma-rays, and conservative estimates of the relevant cross sections. Most of the data in the FMIT activation library has been generated using ENDF/B-V data (when it exists) along with a modified version of the THRESH code. The modification extends the output of THRESH to 40 MeV with normalization to the ENDF/B-V data at 20 MeV whenever possible. More exact treatments, with codes such as HAUSER, are utilized for a limited number of reactions. A few measurements of neutron activation are being planned to provide integral data for direct applications and for verifying calculational techniques.

The current status of calculations have been summarized for activation of stainless steel and other materials within the prime test volume, activation of the beam tube near the lithium target, activation along the LINAC, and activation of air within the accelerator tunnel. The more important reactions were displayed.

The calculation of nuclear heat deposition continues to be a problem due to inaccurate energy balances in ENDF/B and uncertainties in cross section data at higher energies. An important step has been made in a reevaluation of iron by LASL with improved energy balances and gamma production cross sections. A measurement of neutron transmission through an iron block, due to a (d,Li) source, will improve our understanding at the higher energies.

Thick target measurements of the (d,Li) neutron source have established the energy spectrum and yield at ten angles for 35 MeV incident deuterons. Monte Carlo techniques for modeling this anisotropic source, along with three-dimensional models of the test cell geometry, have been used to determine bulk shield thicknesses, neutron streaming through penetrations in the test cell walls, neutron activation, and nuclear heat deposition within the thermal shield.

Source terms due to deuteron loss within the accelerator and beam transport areas are not very well defined. This is primarily due to uncertainties regarding the magnitude of the deuteron loss rather than uncertainties in deuteron activation and neutron production from deuterons incident upon materials.

REFERENCES

1. E. W. POTTMEYER, Jr., "The Fusion Materials Irradiation Test Facility at Hanford", Journal of Nuclear Materials, 85 & 86, 463-465 (1979).

2. M. R. BHAT and S. PEARLSTEIN, editors, "Symposium on Neutron Cross-Sections from 10 to 40 MeV", BNL-NCS-50681, Brookhaven National Laboratory (1977).

3. D. G. DORAN, "Fusion Materials High Energy Neutron Studies — A Status Report", Paper in Session IV of this Symposium.

4. L. L. CARTER and R. J. MORFORD, "Shielding Calculations for the Fusion Materials Irradiation Test Facility", Trans. Am. Nucl. Soc., 30, 618 (1978).

5. R. W. ROUSSIN et al., "Calculations of the Transport of Neutrons and Secondary Gamma Rays Through Concrete for Incident Neutrons in the Energy Range 15 to 75 MeV", Nuclear Engineering and Design, 25, 250 (1973).

6. D. L. JOHNSON et al., "Measurements and Calculations of Neutron Spectra from 35 MeV Deuterons on Thick Lithium for the FMIT Facility", Journal of Nuclear Materials, 85 & 86 (1979). See also paper in Session II of this Symposium, D. L. JOHNSON et al., "Thick Target Neutron Yields and Spectra from the Li(d,xn) Reaction at 35 MeV".

7. LASL GROUP X-6, "MCNP - A General Monte Carlo Code for Neutron and Photon Transport", LA-7396-M, Los Alamos Scientific Laboratory (Revised November 1979).

8. L. L. CARTER and E. D. CASHWELL, "Particle Transport Simulation with the Monte Carlo Method", TID-26607, ERDA Critical Review Series, U. S. Energy Research and Development Administration, Technical Information Center, Oak Ridge, TN (1975).

9. C. I. ZANELLI et al., "Measurements of Neutron Total and Non-elastic Cross Sections for C, O, Ca, and Fe at UC Davis", Paper in Session III of this Symposium.

10. D. C. LARSON et al., "Transmission Measurements Up To 50 MeV for FMIT Design", Paper in Session III of this Symposium.

11. L. L. CARTER et al., "Monte Carlo Applications at Hanford Engineering Development Laboratory", (HEDL-SA-2072-A), Proceedings of a Seminar-Workshop on Theory and Application of Monte Carlo Methods, held at Oak Ridge, Tennessee April 21-23, 1980. To be published as ORNL/RSIC-44.

12. O. L. DEUTSCH and L. L. CARTER, "Simultaneous Global Calculation of Flux and Importance with Forward Monte Carlo", Proceedings of the Fifth International Conference on Reactor Shielding, R. W. Roussin, L. S. Abbott, and D. E. Bartine, editors; Science Press, Princeton (1977).

13. J. S. HENDRICKS and L. L. CARTER, "Computational Benchmark Problem for Deep Penetration in Iron", LA-8193-MS, Los Alamos Scientific Laboratory (1980). Also published in Trans. Am. Nucl. Soc., 33, 663 (1979).

14. W. B. WILSON, "Nuclear Data Development and Shield Design for Neutrons Below 60 MeV", LA-7159-T, Los Alamos Scientific Laboratory (February 1978).

15. R. G. ALSMILLER, JR. and J. BARISH, "NCDATA - Nuclear Collision Data for Nucleon-Nucleus Collisions in the Energy Range 25 to 400 MeV", ORNL-4220, Oak Ridge National Laboratory (1968).

16. R. G. ALSMILLER, JR. and J. BARISH, "Neutron-Photon Multigroup Cross Sections for Neutron Energies $\leq$ 60 MeV" ORNL/TM-6486, Oak Ridge National Laboratory (August 1978). Also published in Nuclear Science and Engineering, 69, 378-388 (1979).

17. "VITAMIN-C, 171 Neutron, 36 Gamma-Ray Group Cross Sections in AMPX and CCCC Interface Formats for Fusion and LMFBR Neutronics", DLC-41, Radiation Shielding Information Center (1977).

18. R. E. MACFARLANE, "Energy Balance of ENDF/B-V", Trans. Am. Nucl. Soc, 33, 681 (1979).

19. E. D. ARTHUR and P. G. YOUNG, "Evaluation of Neutron Cross Sections to 40 MeV for ^{54,56}Fe", Paper in Session V of this Symposium.

20. D. L. JOHNSON et al., "Measurements and Evaluations of Nuclear Data to Support Early Design Needs of the FMIT Facility", Paper in Session IV of this Symposium.

21. S. PEARLSTEIN, "Neutron Induced Reactions in Medium Massed Nuclei", Journal of Nuclear Energy, 27, 81-99 (1973). Updated by Proceedings of the Conference on Nuclear Cross Sections and Technology, Washington, DC (1975), NBS Special Publication number 425, page 324 (1975).

22. F. M. MANN, "HAUSER*5, A Computer Code to Calculate Nuclear Cross Sections", HEDL-TME 78-83, Hanford Engineering Development Laboratory (1979).

TABLE I

MATERIAL CONSTITUENTS FOR ACTIVATION STUDIES

Isotope	Density (atoms/barn-cm)	Isotope	Density (atoms/barn-cm)
Ordinary Concrete			
H 1	.42184-002	Ca 40	.44404-002
O 16	.37482-001	Ca 42	.27230-004
Na 23	.10774-002	Ca 43	.56027-005
Mg 24	.16782-002	Ca 44	.84890-004
Mg 25	.20504-003	Ca 46	.13060-006
Mg 26	.21484-003	Ca 48	.75095-005
Al 27	.30626-002	Ti 46	.11819-004
Si 28	.96644-002	Ti 47	.10317-004
Si 29	.47081-003	Ti 48	.10317-003
Si 30	.31475-003	Ti 49	.73789-005
P 31	.38919-004	Ti 50	.72483-005
S 32	.35784-004	Mn 55	.31801-004
S 33	.35915-006	Fe 54	.11493-003
S 34	.17696-005	Fe 56	.17631-002
K 39	.21484-003	Fe 57	.39115-004
K 41	.14692-004	Fe 58	.51913-005
Stainless Steel			
Cr 50	.70009-003	Fe 57	.12112-002
Cr 52	.12971-001	Fe 58	.16922-003
Cr 53	.14517-002	Co 59	.16321-004
Cr 54	.35906-003	Ni 58	.67174-002
Mn 55	.17266-002	Ni 60	.24825-002
Fe 54	.35305-002	Ni 61	.10308-003
Fe 56	.53773-001	Ni 62	.51884-003
		Ni 64	.80059-004
Aluminum Beam Tube			
Al 27	.58003-01	Cr 53	.10132-04
Mg 24	.52984-03	Cr 54	.29800-05
Mg 25	.69732-04	Mn 55	.88804-04
Mg 26	.69732-04	Fe 54	.17880-04
Si 28	.32005-03	Fe 56	.18297-03
Si 29	.20264-04	Fe 57	.41720-05
Si 30	.10132-04	Fe 58	.59600-06
Ti 46	.41720-05	Cu 63	.39932-04
Ti 47	.41720-05	Cu 65	.19072-04
Ti 48	.38144-04	Zn 64	.29800-04
Ti 49	.29800-05	Zn 66	.17284-04
Ti 50	.29800-05	Zn 67	.29800-05
Cr 50	.47680-05	Zn 68	.11920-04
Cr 52	.91784-04	Zn 70	.59600-06

TABLE I (continued)

Isotope	Density (atoms/barn-cm)	Isotope	Density (atoms/barn-cm)
Iron			
Fe 54	.49184-002	Fe 57	.17808-002
Fe 56	.77846-001	Fe 58	.25440-003
Aluminum			
Al 23	.60300-001		
Copper			
Cu 63	.59275-001	Cu 65	.25610-001
Titanium			
Ti 46	.47061-002	Ti 49	.30618-002
Ti 47	.42525-002	Ti 50	.29484-002
Ti 48	.41788-001		
Sodium			
Na 23	.25400-001		
Cobalt			
Co 59	.91000-001		

TABLE II

IMPORTANT NEUTRON ACTIVATION REACTIONS

Target Material	Major Reactions
Stainless Steel (Test Module)	$^{58}Ni(n,t)^{56}Co$ $^{58}Ni(n,nd)^{56}Co$ $^{58}Ni(n,2np)^{56}Co$ $^{56}Fe(n,p)^{56}Mn$ $^{58}Ni(n,p)^{58}Co$
Aluminum (Beam Tube)	$^{27}Al(n,\alpha)^{24}Na$ $^{24}Mg(n,p)^{24}Na$ $^{66}Zn(n,2n)^{65}Zn$ $^{63}Cu(n,\alpha)^{60}Co$ $^{46}Ti(n,p)^{46}Sc$
Ordinary Concrete (Accelerator Tunnel)	$^{23}Na(n,\gamma)^{24}Na$ $^{24}Mg(n,p)^{24}Na$ $^{27}Al(n,\alpha)^{24}Na$ $^{23}Na(n,2n)^{22}Na$ $^{24}Mg(n,t)^{22}Na$ $^{55}Mn(n,\gamma)^{56}Mn$ $^{54}Fe(n,p)^{54}Mn$ $^{56}Fe(n,t)^{54}Mn$
Air (Accelerator Tunnel)	$^{14}N(n,2n)^{13}N$ $^{16}O(n,p)^{16}N$ $^{14}N(n,p)^{14}C$ $^{40}Ar(n,2n)^{39}Ar$ $^{40}Ar(n,\gamma)^{41}Ar$
Drift Tube and Tank Wall (LINAC)	$^{54}Fe(n,p)^{54}Mn$ $^{56}Fe(n,nd)^{54}Mn$ $^{56}Fe(n,t)^{54}Mn$

TABLE III

NEUTRON ACTIVATION OF STAINLESS STEEL WITHIN PRIME TEST VOLUME

(One Year Irradiation with Target Directly in Front of Beam)

Major Reactions	Percentage Contribution To Total	Decay Rate (Curies/cm^3) At Shutdown	Decay Rate (Curies/cm^3) 7 Days Cooling	Dominant Gamma Energies (MeV)	Half-Life (Days)
$^{56}Fe(n,p)^{56}Mn$	97			1.81(29%)	
Total ^{56}Mn		23.3	~0.	2.11(15%)	0.108
$^{58}Ni(n,p)^{58}Co$	98			0.81(99%)	
Total ^{58}Co		22.7	21.2	1.67(0.6%)	71.
$^{55}Mn(n,2n)^{54}Mn$	25				
$^{54}Fe(n,p)^{54}Mn$	55				
$^{56}Fe(n,t)^{54}Mn$	12				
Total ^{54}Mn		9.65	9.50	0.84(100%)	300.
$^{58}Ni(n,nd)^{56}Co$	10			2.02(11%)	
$^{58}Ni(n,t)^{56}Co$	90			2.60(17%)	
Total ^{56}Co		0.159	0.150	3.26(13%)	77.
$^{60}Ni(n,p)^{60}Co$	92			1.17(100%)	
Total ^{60}Co		0.22	0.21	1.33(100%)	1934.
$^{58}Ni(n,p)^{57}Co$	68				
$^{58}Ni(n,d)^{57}Co$	30				
Total ^{57}Co		1.94	1.91	0.69(14%)	270
$^{58}Ni(n,2n)^{57}Ni$	100			1.37(86%)	
Total ^{57}Ni		1.12	0.039	1.89(14%)	1.5
$^{50}Cr(n,nd)^{48}V$	20				
$^{50}Cr(n,t)^{48}V$	80			1.31(97%)	
Total ^{48}V		0.260	0.193	2.24(3%)	16.2
$^{54}Fe(n,nd)^{52}Mn$	26				
$^{54}Fe(n,t)^{52}Mn$	73			0.94(84%)	
Total ^{52}Mn		0.263	0.111	1.43(100%)	5.6

TABLE IV

NEUTRON ACTIVATION OF ELEMENTS WITHIN PRIME TEST VOLUME

(One Year Irradiation with Target Directly in Front of Beam)

Major Reactions	Percentage Contribution To Total	Decay Rate (Curies/cm^3) At Shutdown	Decay Rate (Curies/cm^3) 7 Days Cooling	Dominant Gamma Energies (MeV)	Half-Life (Days)
IRON					
$^{56}Fe(n,p)^{56}Mn$	98			1.81(29%)	
Total ^{56}Mn		33.6	~0.	2.11(15%)	0.108
$^{54}Fe(n,p)^{54}Mn$	73				
$^{56}Fe(n,t)^{54}Mn$	17				
Total ^{54}Mn		10.3	10.1	0.84(100%)	300.
$^{54}Fe(n,nd)^{52}Mn$	26				
$^{54}Fe(n,t)^{52}Mn$	73			0.94(85%)	
Total ^{52}Mn		0.365	0.156	1.43(100%)	5.7
$^{58}Fe(n,\gamma)^{59}Fe$	100			1.10(56%)	
Total ^{59}Fe		0.014	0.013	1.29(44%)	45.
ALUMINUM					
$^{27}Al(n,p)^{27}Mg$	100			0.84(70%)	
Total ^{27}Mg		28.6	~0.	1.01(30%)	0.007
$^{27}Al(n,\alpha)^{24}Na$	100			1.37(100%)	
Total ^{24}Na		28.3	0.012	2.75(100%)	0.630
COPPER					
$^{65}Cu(n,2n)^{64}Cu$	96			0.51(38%)	
Total ^{64}Cu		77.2	0.0097	1.34(0.5%)	0.54
$^{65}Cu(n,p)^{65}Ni$	100			1.12(16%)	
Total ^{65}Ni		8.08	~0.	1.48(25%)	0.106
$^{63}Cu(n,\alpha)^{60}Co$	98			1.17(100%)	
Total ^{60}Co		1.44	1.43	1.33(100%)	1934.
SODIUM					
$^{23}Na(n,2n)^{22}Na$	100			0.51(180%)	
Total ^{22}Na		2.41	2.39	1.28(100%)	949.
$^{23}Na(n,\gamma)^{24}Na$	100			1.37(100%)	
Total ^{24}Na		0.069	0.00003	2.75(100%)	0.63

TABLE IV (continued)

Major Reactions	Percentage Contribution To Total	Decay Rate (Curies/cm³) At Shutdown	Decay Rate (Curies/cm³) 7 Days Cooling	Dominant Gamma Energies (MeV)	Half-Life (Days)
NICKEL					
$^{58}Ni(n,nd)^{56}Co$	10			2.02(11%)	
$^{58}Ni(n,t)^{56}Co$	90			2.60(17%)	
Total ^{56}Co		1.48	1.39	3.26(13%)	77.
$^{60}Ni(n,p)^{60}Co$	93			1.17(100%)	
Total ^{60}Co		2.02	2.02	1.33(100%)	1934.
$^{60}Ni(n,2p)^{59}Fe$	55				
$^{62}Ni(n,\alpha)^{59}Fe$	45			1.10(56%)	
Total ^{59}Fe		0.91	0.81	1.29(44%)	45.
$^{58}Ni(n,p)^{58}Co$	100			0.81(99%)	
Total ^{58}Co		210.7	197.0	1.67(0.6%)	71.
TITANIUM					
$^{47}Ti(n,np)^{46}Sc$	18				
$^{46}Ti(n,p)^{46}Sc$	65				
$^{48}Ti(n,t)^{46}Sc$	11				
Total ^{46}Sc		9.82	9.27	1.12(100%)	84.
$^{48}Ti(n,p)^{48}Sc$	87			1.04(100%)	
Total ^{48}Sc		11.1	0.77	1.31(100%)	1.8
$^{48}Ti(n,2p)^{47}Ca$	62				
$^{50}Ti(n,\alpha)^{47}Ca$	33				
Total ^{47}Ca		0.79	0.27	1.31(74%)	4.5
COBALT					
$^{59}Co(n,2n)^{58}Co$	100			0.81(99%)	
Total ^{58}Co		216.	201.	1.67(0.6%)	71.
$^{59}Co(n,p)^{59}Fe$	100			1.10(56%)	
Total ^{59}Fe		23.2	20.8	1.29(44%)	45.
$^{59}Co(n,\alpha)^{56}Mn$	100			1.81(29%)	
Total ^{56}Mn		9.49	~0.	2.11(15%)	0.108
$^{59}Co(n,\gamma)^{60}Co$	100			1.17(100%)	
Total ^{60}Co		0.71	0.71	1.33(100%)	1934.

TABLE V

NEUTRON ACTIVATION WITHIN CONCRETE WALLS OF ACCELERATOR TUNNEL

(For 3 μA/m Deuteron Loss)

Major Reactions	Percentage Contribution To Total	Decay Rate (Curies/cm³)[a] At Shutdown	Decay Rate (Curies/cm³)[a] 24 Hours Cooling	Dominant Gamma Energies (MeV)	Half-Life (Days)
$^{23}Na(n,\gamma)^{24}Na$	83.2				
$^{24}Mg(n,p)^{24}Na$	10.2				
$^{27}Al(n,\alpha)^{24}Na$	5.8			1.37(100%)	
Total ^{24}Na		3.5×10^{-9}	1.2×10^{-9}	2.75(100%)	0.630
$^{55}Mn(n,\gamma)^{56}Mn$	96.3			0.85(99%)	
$^{56}Fe(n,p)^{56}Mn$	3.6			1.81(29%)	
Total ^{56}Mn		3.0×10^{-9}	4.9×10^{-12}	2.11(15%)	0.108
$^{54}Fe(n,p)^{54}Mn$	60.8				
$^{56}Fe(n,t)^{54}Mn$	21.6				
Total ^{54}Mn		7.8×10^{-11}	7.8×10^{-11}	0.84(100%)	312.
$^{24}Mg(n,t)^{22}Na$	53.7				
$^{23}Na(n,2n)^{22}Na$	41.5			0.51(180%)	
Total ^{22}Na		2.6×10^{-11}	2.6×10^{-11}	1.28(100%)	956.

[a] Near surface of concrete at high energy end of LINAC.

TABLE VI

NEUTRON ACTIVATION WITHIN DRIFT TUBE AND TANK OF LINAC

(For 3 μA/m Deuteron Loss)

Activation Nuclides	Decay Rate After 24 Hours Cooling		Dominant Gamma Energies (MeV)	Half-Life (Days)
	Drift Tube [a] (Curies)	Tank Wall [a] (Curies)		
^{54}Mn	3.32×10^{-2}	3.74×10^{-3}	0.84(100%)	312.
^{52}Mn	1.41×10^{-3}	1.82×10^{-4}	0.94(85%) 1.43(100%)	5.7
^{56}Mn	3.6×10^{-5}	5.5×10^{-6}	0.85(99%) 1.81(29%) 2.11(15%)	0.108
^{60}Co	2.30×10^{-3}	3.40×10^{-4}	1.17(100%) 1.33(100%)	1934.
^{64}Cu	5.43×10^{-3}	6.51×10^{-3}	0.51(38%) 1.34(0.5%)	0.54
^{58}Co	1.94×10^{-3}	---	0.81(99%) 1.67(0.6%)	71.
^{56}Co	1.71×10^{-4}	---	2.02(11%) 2.60(17%) 3.26(13%)	77.
^{59}Fe	---	1.92×10^{-4}	1.10(56%) 1.29(44%)	45.

[a] Activation of material along a 69.7 cm length at high energy end of LINAC. The FMIT activation library has been updated since this table was generated.

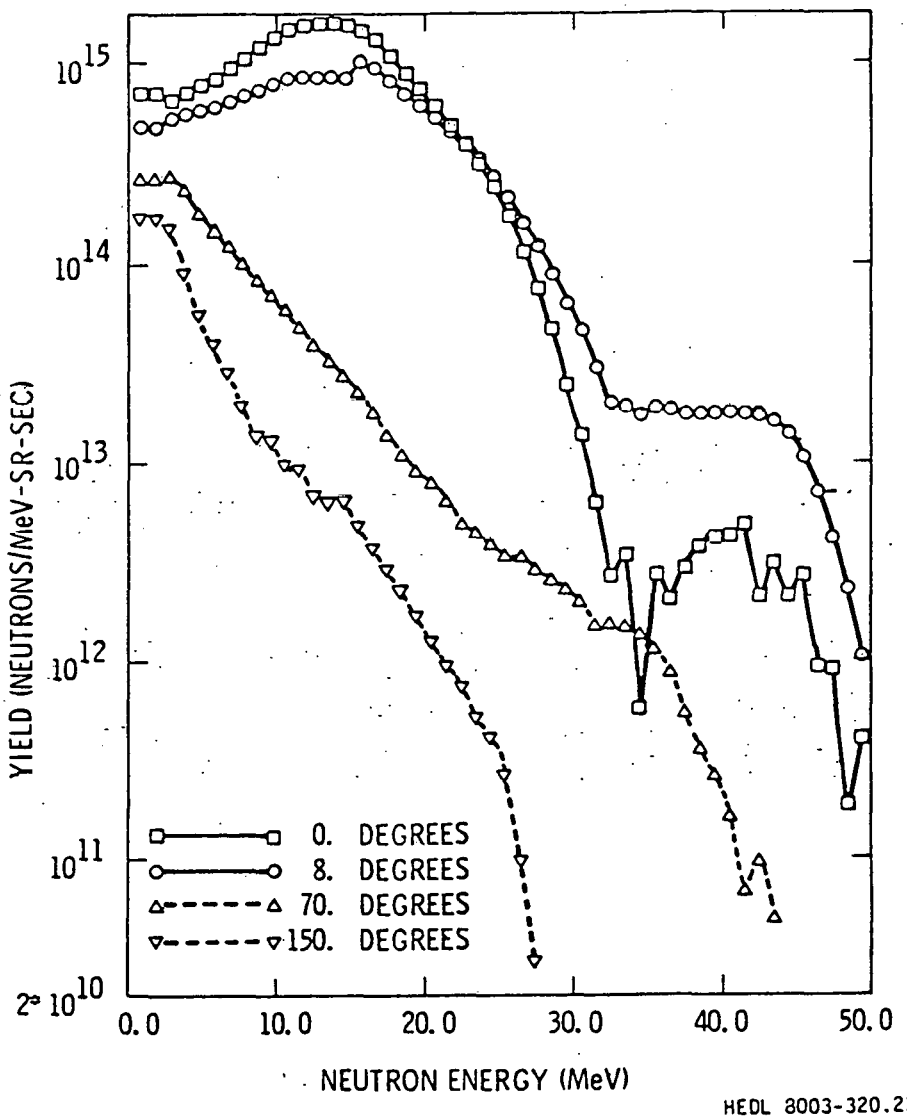

Figure 1. Neutron spectra from a 0.1 Amp current of 35 MeV deuterons incident upon lithium.

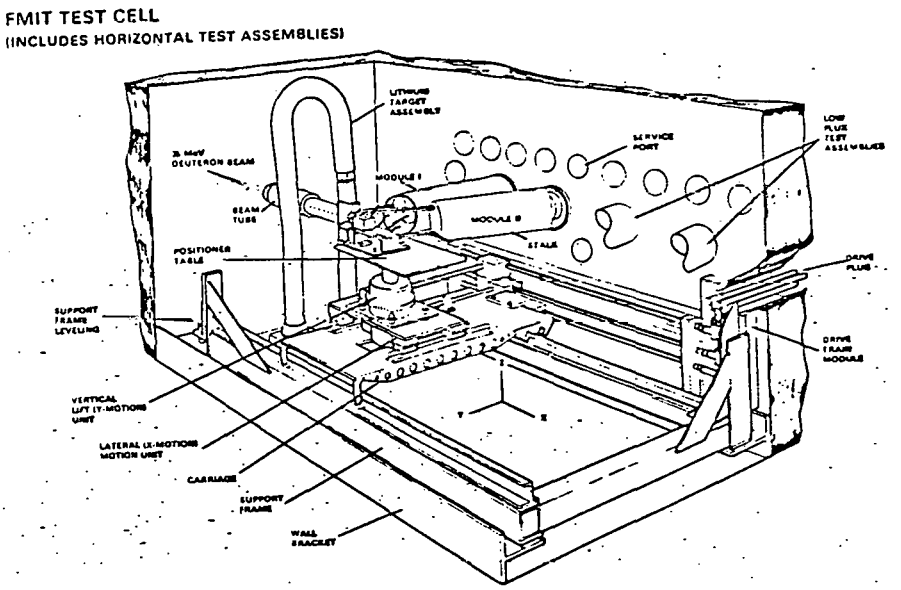

Figure 2a. Conceptual arrangement of four horizontal test assemblies and a vertical test assembly in the FMIT test cell.

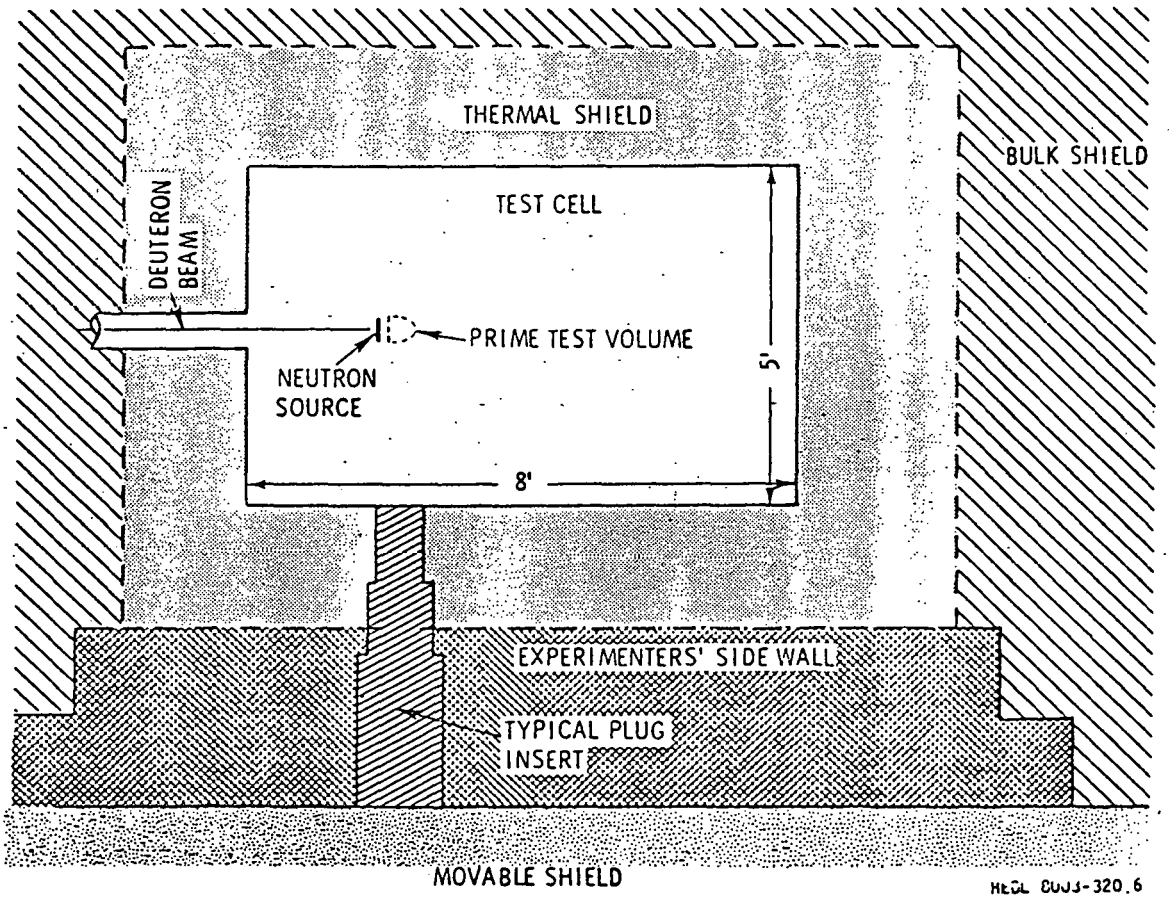

Figure 2b. Plan view of empty test cell.

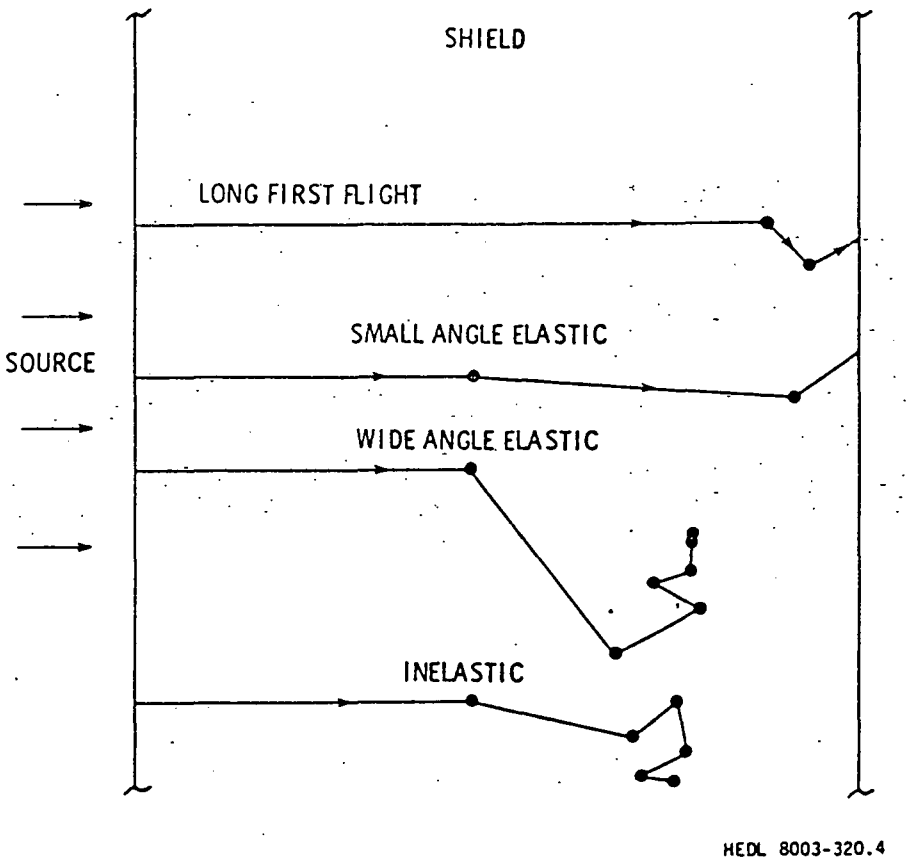

Figure 3. Penetration of neutrons through a shield for a 20 to 50 MeV incident source.

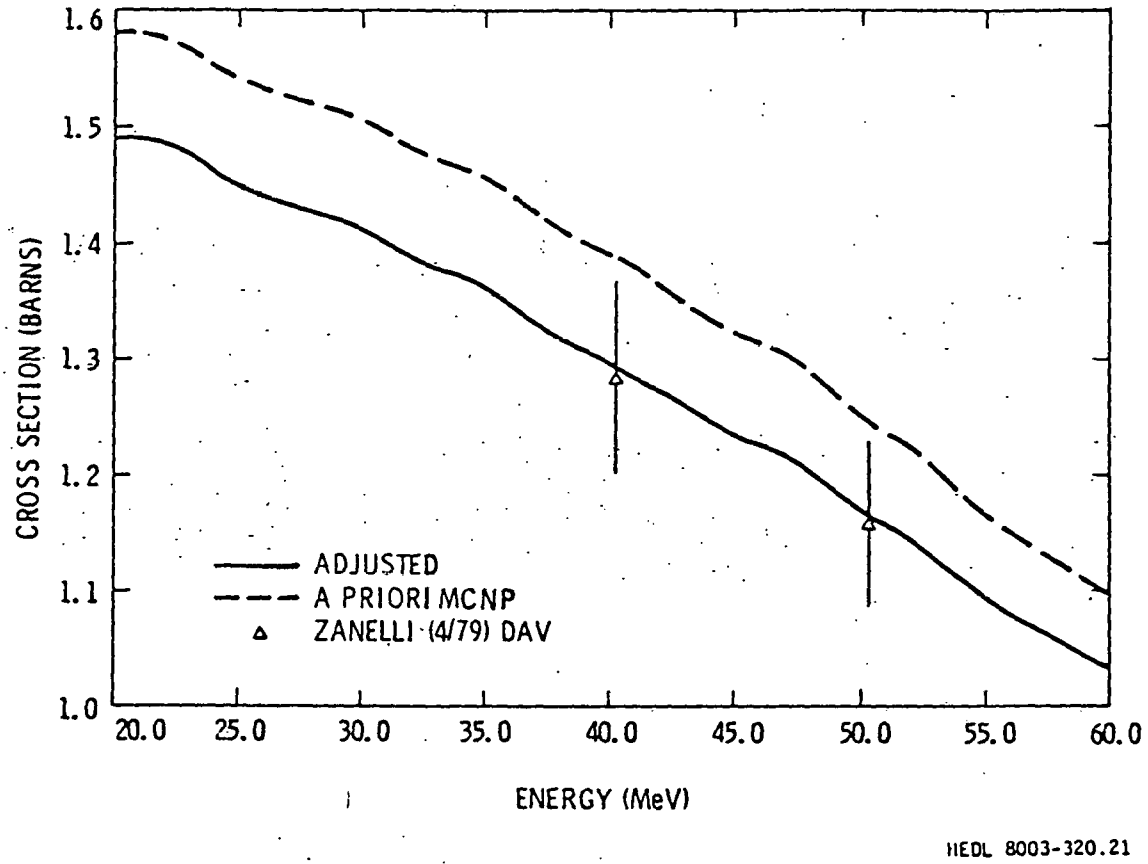

Figure 4. Removal cross section for two evaluations of iron.

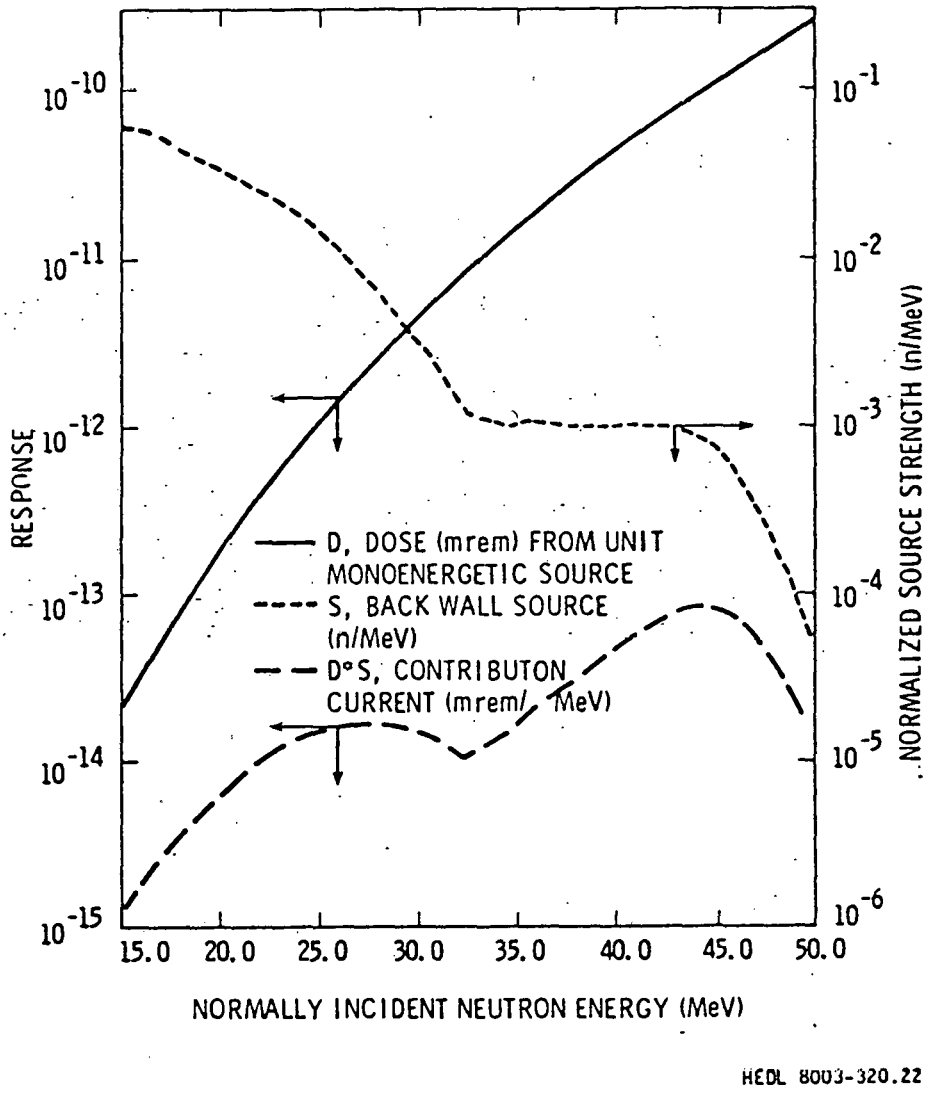

Figure 5. Dose and contribution current through 8 ft of high density concrete. (3.6 g/cm^3)

	SOURCE OF NUCLEAR DATA
POINTWISE CROSS SECTIONS FOR MCNP MONTE CARLO CODE	
<20 MeV neutron energy including photon production	ENDF/B-IV
20 MeV to 60 MeV (H, C, O, Si, Ca, Cr, Fe, Ni)	
Nonelastic	Ref. 14; based upon optical model [a]
Nonelastic energy-angle distribution	Ref. 15; based upon IC+E
Elastic	Optical model [b]
Elastic angular distribution	Optical model [b]
Gamma production	Ratio of gamma production to total assumed constant above 20 MeV
MULTIGROUP P_5 COUPLED NEUTRON-GAMMA [c]	
(Elements H, ^{10}B, ^{11}B, C, O, Si, Ca, Cr, Fe, Ni)	
<14.9 MeV neutron energy	RSIC fusion cross section library; Ref. 17
14.9 MeV to 60 MeV	
Nonelastic	Ref. 16; optical model
Nonelastic energy-angle distribution	Ref. 15, 16; based upon IC+E
Elastic	Ref. 16; optical model
Elastic angular distribution	Ref. 16; optical model
Gamma production	None above 14.9 MeV

[a] The nonelastic cross section for Ca was based upon the IC+E model.

[b] Hydrogen cross sections above 20 MeV based upon measured values.

[c] 47 neutron groups and 21 gamma groups.

Figure 6. Cross section libraries for FMIT.

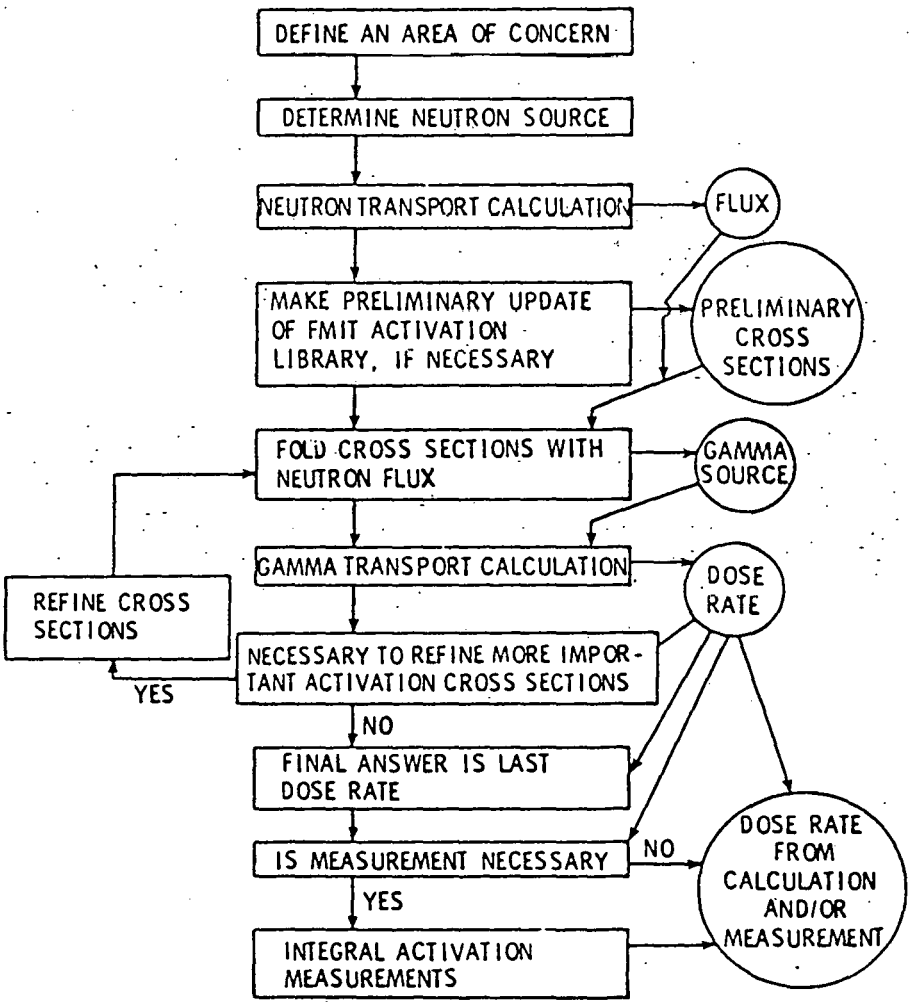

Figure 7. Calculation of neutron activation.

ATTENDEES TO THE SYMPOSIUM ON NEUTRON CROSS SECTIONS FROM 10-50 MEV May 12-14, 1980

*

DR.R.G. ALSMILLER JR
OAK RIDGE NATIONAL LAB
P.O.BOX X
OAK RIDGE, TENNESSEE 37830

*

DR.E.D. ARTHUR
LOS ALAMOS SCIENTIFIC LAB.
T-2 MS-243
P.O.BOX 1663
LOS ALAMOS, NM 87545

*

DR.G.S.BAUER
INST.FUR FESKORPERFORSCHUNG
KERNFORSCHUNGSANLAGE JULICH
GMBH
D-5170 JULICH POSTFACH 1913
WEST GERMANY

*

DR.ZANE W.BELL
OAK RIDGE NATL LAB
P.O.BOX X
OAK RIDGE,TN 37830

*

DR.M.R.BHAT
BLDG. 197D
NATIONAL NUCLEAR DATA CENTER
BROOKHAVEN NATIONAL LAB
UPTON,L.I.N.Y. 11973

*

DR.C.D.BOWMAN
RADIATION DIV
ROOM B119 BLDG245
NATIONAL BUREAU OF STDS
WASHINGTON, DC 20234

*

DR.DAVID BRENNER
LOS ALAMOS SCIENTIF LAB
MS-809,P.O.BOX 1663
LOS ALAMOS,NM 87545

*

DR. J.C. BROWNE
LOS ALAMOS SCIENTIFIC LAB.
P-3 MS-442
P.O.BOX 1663
LOS ALAMOS, NM 87545

*

DR.T.W.BURROUS
BLDG. 197D
NATIONAL NUCLEAR DATA CENTER
BROOKHAVEN NATIONAL LAB
UPTON,L.I.N.Y. 11973

*

DR.ALLAN D.CARLSON
RADIATION PHYSICS BLDG
ROOM B119
NATL BUREAU OF STANDARDS
WASHINGTON, DC 20234

*

DR.JOHN M.CARPENTER
BUILDING 372
ARGONNE NATIONAL LAB
9700 SOUTH CASS AVE
ARGONNE,IL 60439

*

DR.L.CARTER
WESTINGHOUSE HANFORD
P.O.BOX 1970,/B-47
RICHLAND,WA 99352

*

DR.R.E.CHRIEN
BLDG 510A
PHYSICS DEPT
BROOKHAVEN NATL LAB
UPTON,L.I.N.Y. 11973

*

DR. S.W. CIERJACKS
INST. FUER ANGEWANDTE
KERNPHYSIK
KERNFORSCHUNGSZENTRUM
KARLSRUHE
POSTFACH 3640
D-7500 KARLSRUHE
WEST GERMANY

*

DR.J.JOSEPH COYNE
NAT'L BUREAU OF STANDARDS
CENTER FOR RADIATION
RESEARCH
WASHINGTON,DC 20234

*

PROF.RONALD Y.CUSSON
DUKE UNIVERSITY
PHYSICS DEPT
DURHAM NC 27706

*

DR.G.F.DELL
BLDG 510B,PHYSICS DEPT.
20 PENNSYLVANIA AVE.
BROOKHAVEN NATL LAB
UPTON,LI NY 11973

*

DR.P.J.DIMBYLOW
NATIONAL RADIOLOGICAL
PROTECTION BOARD
HARWELL,DIDCOT,OXON,OX11 ORQ
UNITED KINGDOM

*
DR.M.DIVADEENAM
BLDG. 197D
NATIONAL NUCLEAR DATA CENTER
BROOKHAVEN NATIONAL LAB
UPTON,L.I.N.Y. 11973

*
M.W.FANELLI
BLDG. 197D
NATIONAL NUCLEAR DATA CENTER
BROOKHAVEN NATIONAL LAB
UPTON,L.I.N.Y. 11973

*
DR.R.W. FINLAY
DEPT. OF PHYSICS
OHIO UNIVERSITY
ATHENS,OH 45701

*
DR.C.Y. FU
OAK RIDGE NATIONAL LAB
P.O.BOX X
OAK RIDGE, TENNESSEE 37830

*
DR.MAUREEN A.GARDNER
LAWRENCE LIVERMORE LAB
P.O.BOX 808
LIVERMORE,CA 94550

*
DR.P.GRAND
BLDG.129
DEPT.OF NUCLEAR ENERGY
BROOKHAVEN NATIONAL LAB
UPTON,L.I.N.Y. 11973

*
DR. D. DORAN
HANFORD ENGINEERING DEVELOPMENT
LAB
P.O.BOX 1970
RICHLAND, WASHINGTON 99352

*
DR. H. FARRAR IV
COMPONENT ENG AND TECH DIV
NORTH AMERICAN ROCKWELL
P.O. 309
8900 DE SOTO AVE
CANOGA PARK, CAL 91304

*
DR.JOHN S.FRASER
CHALK RIVER NUCLEAR LAB
ATOMIC ENERGY OF CANADA LTD
CHALK RIVER
ONTARIO KOJ1JO,CANADA

*
DR.R.C.FULLER
BLDG.197C
DEPT.OF NUCLEAR ENERGY
BROOKHAVEN NATIONAL LAB
UPTON,L.I.N.Y. 11973

*
DR.A.N.GOLAND
BLDG.510B
PHYSICS DEPT
BROOKHAVEN NATIONAL LAB
UPTON,L.I.N.Y. 11973

*
DR.LAWRENCE GREEN
WESTINGHOUSE FUSION
POWER SYSTEM
PITTSBURG,USA

*
DR.C.L.DUNFORD
BLDG. 197D
NATIONAL NUCLEAR DATA CENTER
BROOKHAVEN NATIONAL LAB
UPTON,L.I.N.Y. 11973

*
DR.A.T.G.FERGUSON
NUC.PHYS.DIV.HANGAR 8
A.E.R.E
HARWELL,DIDCOT,OXON,OX11 ORA
UNITED KINGDOM

*
DR.J.FREHAUT
CEA-DAM
CENTRE DETUDES DE
BRUYERS LE CHATEL
SERVICE DE PHYSIQUE NUCLEAIRE
B.P.NO.561
92542 MONTROUGE CEDEX
FRANCE

*
DR.D. GARDNER
LAWRENCE LIVERMORE LAB
P.O.BOX 808
LIVERMORE, CALIF.94550

*
DR.R. GOLD
HANFORD ENGINEERING DEVELOPMENT
LAB
P.O.BOX 1970, /C-39
RICHLAND, WASHINGTON 99352

*
DR.L.R. GREENWOOD
ARGONNE NAT'L LAB.
9700 SOUTH CASS AVE
ARGONNE,IL 60439

*

DR.H.GRUPPELAAR
NETHERLANDS ENERGY RES.FOUNDN
P.O.BOX 1
1755ZG PETTEN,THE NETHERLANDS

*

DR.L.F. HANSEN
LAWRENCE LIVERMORE LAB
P.O.BOX 808
LIVERMORE, CALIF.94550

*

DR.N.E.HOLDEN
BLDG. 197D
NATIONAL NUCLEAR DATA CENTER
BROOKHAVEN NATIONAL LAB
UPTON,L.I.N.Y. 11973

*

DR.R.G.JOHNSON
RADP B119
NATIONAL BUREAU OF STANDARDS
WASHINGTON,DC 20234

*

DR.R.R.KINSEY
BLDG. 197D
NATIONAL NUCLEAR DATA CENTER
BROOKHAVEN NATIONAL LAB
UPTON,L.I.N.Y. 11973

*

DR.J.J.KUKKONEN
BLDG.130
DEPT.OF NUCLEAR ENERGY
BROOKHAVEN NATIONAL LAB
UPTON,L.I.N.Y. 11973

*

DR.M. GUINAN
LAWRENCE LIVERMORE LAB
P.O.BOX 808
LIVERMORE, CA 94550

*

DR.DALE W.HEIKKINEN
LAWRENCE LIVERMORE LAB
P.O.BOX 808 L-397
LIVERMORE,CA 94550

*

DR.R.J.HOWERTON
L-71
LAWRENCE LIVERMORE LAB
P.O.BOX 808
LIVERMORE,CA 94550

*

DR.CONSTANCE KALBACH
TRIANGLE UNIVERSITIES NUC.LAB
PHYSICS DEPT
DUKE UNIVERSITY
DURHAM, NC 27706

*

DR.D.W.KNEFF
COMPONENT ENG AND TECH DIV
NORTH AMERICAN ROCKWELL
P.O. 309
8900 DE SOTO AVE
CANOGA PARK,CAL 91304

*

DR.R.J.LABAUVE
T-2 MS-243
LOS ALAMOS SCIENTIFIC LAB
P.O.BOX 1663
LOS ALAMOS,NM 87545

*

DR.R.C. HAIGHT
LAWRENCE LIVERMORE LAB L-405
P.O.BOX 808
LIVERMORE, CALIF.94550

*

DR.M.HILLMAN
BLDG 815
DEPT.OF ENERGY AND ENVRNMNT
BROOKHAVEN NATIONAL LAB
UPTON,L.I.N.Y. 11973

*

DR.D.L.JOHNSON
WESTINGHOUSE HANFORD
P.O.BOX 1970
RICHLAND,WA 99352

*

DR.WALTER KATO
BLDG 130
DEPT.OF NUCLEAR ENERGY
BROOKHAVEN NATIONAL LAB
UPTON,L.I.N.Y. 11973

*

DR.H.J.C.KOUTS
BLDG 197C
DEPT.OF NUCLEAR ENERGY
BROOKHAVEN NATL LAB
UPTON,L.I.N.Y. 11973

*

DR.DUANE LARSON
NEUTRON PHYSICS BLDG 6010
OAKRIDGE NATIONAL LAB
P.O.BOX X
OAK RIDGE,TN 37830

*
O.W.LAZARETH JR.
BLDG 129
DEPT.OF NUCLEAR ENERGY
BROOKHAVEN NATL LAB
UPTON,L.I.N.Y. 11973

*
DR.P.W.LISOWSKI
LOS ALAMOS SCIENTIFIC LAB
M.S-442
P.O.BOX 1663
LOS ALAMOS,NM 87545

*
DR. F.M. MANN
ROOM 143
FEDERAL BUILDING
WESTINGHOUSE HANFORD
P.O. BOX 1970
RICHLAND, WASHINGTON 99352

*
DR.SOPHIE MOORE
BLDG. 197D
NATIONAL NUCLEAR DATA CENTER
BROOKHAVEN NATIONAL LAB
UPTON,L.I.N.Y. 11973

*
DR.DAVID R.NETHAWAY
LAWRENCE LIVERMORE LAB
P.O.BOX 808
LIVERMORE,CA 94550

*
DR.S.PEARLSTEIN
BLDG. 197D
NATIONAL NUCLEAR DATA CENTER
BROOKHAVEN NATIONAL LAB
UPTON,L.I.N.Y. 11973

*
DR.J.R.LEMLEY
BLDG.197C
DEPT.OF NUCLEAR ENERGY
BROOKHAVEN NATIONAL LAB
UPTON,L.I.N.Y. 11973

*
DR. M.A. LONE
CHALK RIVER NUCLEAR LAB.
ATOMIC ENERGY OF CANADA LTD.
CHALK RIVER
ONTARIO KOJ1JO
CANADA

*
DR.JOSEPH C.MCDONALD
MEM.SLOAN-KETTERING
CANCER CENTER
1275 YORK AVE
NEW YORK,NY 10021

*
DR.S.F.MUGHABGHAB
BLDG. 197D
NATIONAL NUCLEAR DATA CENTER
BROOKHAVEN NATIONAL LAB
UPTON,L.I.N.Y. 11973

*
DR.CLAES NORDBORG
NEA DATA BANK
BAT45,BP NO 9
F-91190 GIF-SUR-YVETTE
FRANCE

*
DR.R.W.PEELLE
NEUTRON PHYSICS DIV
OAK RIDGE NATL LAB
P.O.BOX X,BLDG 6010
OAK RIDGE,TN 37830

*
DR.B.R.LEONARD JR
BATTELLE NORTHWEST
P.O.BOX 999
RICHLAND,WASH. 99352

*
DR.B.A.MAGURNO
BLDG. 197D
NATIONAL NUCLEAR DATA CENTER
BROOKHAVEN NATIONAL LAB
UPTON,L.I.N.Y. 11973

*
V.L.MCLANE
BLDG. 197D
NATIONAL NUCLEAR DATA CENTER
BROOKHAVEN NATIONAL LAB
UPTON,L.I.N.Y. 11973

*
DR.D.W.MUIR
LAS ALAMOS SCIENTIFIC LAB
T-2,MS-243
P.O.BOX 1663
LOS ALAMOS,NM 87545

*
DR.B.D.PATE
TRIUMF
UNIV.OF BRITISH COLUMBIA
4004 WESTBROOK MALL
VANCOUVER,BC V6T 2A3
BRITISH COLUMBIA,CANADA

*
DR.L.K.PEKER
BLDG. 197D
NATIONAL NUCLEAR DATA CENTER
BROOKHAVEN NATIONAL LAB
UPTON,L.I.N.Y. 11973

*

DR.F.G.J.PEREY
OAK RIDGE NATIONAL LAB
P.O.BOX X
OAK RIDGE,TN 37830

*

DR.HANS G.PRIESMEYER
INST.F.KERNPHYSIK
UNIV. KIEL
D-2054,GEESTHACHT
W.GERMANY

*

DR.G.RANDERS-PEHRSON
DEPT.OF PHYSICS
OHIO UNIVERSITY
ATHENS,OH 45701

*

DR.URI SALMI
RACAH INST.OF PHYSICS
HEBREW UNIV.OF JERUSALEM
JERUSALEM,ISRAEL

*

DR.A.B. SMITH
ARGONNE NATIONAL LAB.
9700 SOUTH CASS AVE.
ARGONNE, ILLINOIS 60439

*

DR.LEONA STEWART
ROOM203,BLDG.6010
OAK RIDGE NATIONAL LAB
P.O.BOX X
OAK RIDGE,TN 37830

*

DR.CLAUDE PHILIS
CEA-DAM
CENTRE DETUDES DE
BRUYERES LE CHATEL
SERVICE DE PHYSIQUE NUCLEAIRE
B.P.NO.561
92542 MONTROUGE CEDEX
FRANCE

*

DR.A.PRINCE
BLDG. 197D
NATIONAL NUCLEAR DATA CENTER
BROOKHAVEN NATIONAL LAB
UPTON,L.I.N.Y. 11973

*

DR.P.ROSE
BLDG. 197D
NATIONAL NUCLEAR DATA CENTER
BROOKHAVEN NATIONAL LAB
UPTON,L.I.N.Y. 11973

*

MRS.F.M.SCHEFFEL
BLDG. 197D
NATIONAL NUCLEAR DATA CENTER
BROOKHAVEN NATIONAL LAB
UPTON,L.I.N.Y. 11973

*

DR.J.STEHN
BLDG. 197D
NATIONAL NUCLEAR DATA CENTER
BROOKHAVEN NATIONAL LAB
UPTON,L.I.N.Y. 11973

*

DR.BRIGITTE STROHMAIER
INST.FUR RADIUMFORSCHUNG
UNIV.WIEN
BOLTZMANNGASSE 3
A-1090 WIEN
AUSTRIA

*

DR.T.W.PHILLIPS
LAWRENCE LIVERMORE LAB
P.O.BOX 808
LIVERMORE,CA 94550

*

DR.S.M. QAIM
INSTITUT FUR CHEMIE DER
KERNFORSHUNGSANLAGE JULICH GMBH
INSTITUTE 1 NUKLEARCHEMIE
D-5170 JULICH W.GERMANY

*

DR.GARY J.RUSSELL
LOS ALAMOS SCIENTIFIC LAB
GROUP-P-9,MS-805,PHYSICS DIV
P.O.BOX 1663
LOS ALAMOS,NM 87545

*

DR.R.E.SCHENTER
/A-4
WESTINGHOUSE HANFORD
P.O.BOX 1970
RICHLAND,WA 99352

*

DR.M.L.STELTS
BLDG. 510A
PHYSICS DEPT
BROOKHAVEN NATIONAL LAB
UPTON,L.I.N.Y. 11973

*

DR.T.S.SUBRAMANIAN
BLDG 29,RM-215
LAWRENCE BERKELEY LAB
BERKELEY CA 94720

*
DR. HIROSHI TAKAHASHI
BLDG. 130
DEPT. OF APPLIED SCIENCE
BROOKHAVEN NATIONAL LABORATORY
UPTON, NY 11973

*
DR.SHIGEYA TANAKA
NUCLEAR DATA CENTER
JAERI
TOKAI-MURA IBARAKI-KEN 319-11
JAPAN

*
DR.J.K.TULI
BLDG. 197D
NATIONAL NUCLEAR DATA CENTER
BROOKHAVEN NATIONAL LAB
UPTON,L.I.N.Y. 11973

*
PROF.H.K.VONACH
INST. FUER RADIUMFORSCHUNG
UND KERNPHYSIK
BOLTZMANNGASSE 3
A-1090 WIEN
AUSTRIA

*

PROF.R.L.WALTER
DEPT.OF PHYSICS
DUKE UNIV.
DURHAM,NC 27706

*
DR.P.G.YOUNG
T-2,MS-243
LOS ALAMOS SCIENTIFIC LAB
P.O.BOX 1663
LOS ALAMOS, NM 87545

*

*

*